

94  
4-5-80  
JAC

LA-8408

Lh. 1935

## A Numerical Model of the Gap Test

MASTER

University of California



**LOS ALAMOS SCIENTIFIC LABORATORY**

Post Office Box 1663 Los Alamos, New Mexico 87545

DISTRIBUTED

UNLIMITED

## **DISCLAIMER**

**This report was prepared as an account of work sponsored by an agency of the United States Government. Neither the United States Government nor any agency thereof, nor any of their employees, makes any warranty, express or implied, or assumes any legal liability or responsibility for the accuracy, completeness, or usefulness of any information, apparatus, product, or process disclosed, or represents that its use would not infringe privately owned rights. Reference herein to any specific commercial product, process, or service by trade name, trademark, manufacturer, or otherwise does not necessarily constitute or imply its endorsement, recommendation, or favoring by the United States Government or any agency thereof. The views and opinions of authors expressed herein do not necessarily state or reflect those of the United States Government or any agency thereof.**

---

## **DISCLAIMER**

**Portions of this document may be illegible in electronic image products. Images are produced from the best available original document.**

This work was supported by the US Department of  
the Navy, Strategic Systems Project Office.

Edited by Karyn Ames

**DISCLAIMER**

This report was prepared as an account of work sponsored by an agency of the United States Government. Neither the United States Government nor any agency thereof, nor any of their employees, makes any warranty, express or implied, or assumes any legal liability or responsibility for the accuracy, completeness, or usefulness of any information, apparatus, product, or process disclosed, or represents that its use would not infringe privately owned rights. Reference herein to any specific commercial product, process, or service by trade name, trademark, manufacturer, or otherwise, does not necessarily constitute or imply its endorsement, recommendation, or favoring by the United States Government or any agency thereof. The views and opinions of authors expressed herein do not necessarily state or reflect those of the United States Government or any agency thereof.

**UNITED STATES  
DEPARTMENT OF ENERGY  
CONTRACT W-7405-ENG. 36**

LA-8408

UC-45

Issued: October 1980

# A Numerical Model of the Gap Test

Allen L. Bowman  
James D. Kershner  
Charles L. Mader

## DISCLAIMER

This book was prepared as an account of work sponsored by an agency of the United States Government. Neither the United States Government nor any agency thereof, nor any of their employees, makes any warranty, express or implied, or assumes any legal liability or responsibility for the accuracy, completeness, or usefulness of any information, apparatus, product, or process disclosed, or represents that its use would not infringe privately owned rights. Reference herein to any specific commercial product, process, or service by trade name, trademark, manufacturer, or otherwise, does not necessarily constitute or imply its endorsement, recommendation, or favoring by the United States Government or any agency thereof. The views and opinions of authors expressed herein do not necessarily state or reflect those of the United States Government or any agency thereof.

LAS

48

# A NUMERICAL MODEL OF THE GAP TEST

by

Allen L. Bowman, James D. Kershner, and Charles L. Mader

## ABSTRACT

The Los Alamos Scientific Laboratory (LASL) standard gap test and the Naval Ordnance Laboratory (NOL) large-scale gap test are modeled numerically using the LASL reactive hydrodynamic code 2DE with Forest Fire burn rates. The model shows good agreement between calculated and experimental values for PBX-9404 and TATB (LASL), and VTQ-2 and Composition B (NOL). The calculations demonstrate the two-dimensional nature of the gap tests. This is particularly evident from the calculated distances of run to detonation in the test samples, which are significantly longer than those from the Pop plots at induced pressures near the critical gap length.

---

## I. INTRODUCTION

The relative shock sensitivities of explosive compositions are commonly assessed by means of gap tests. In these tests the shock from a standard donor explosive is transmitted to the test explosive through an inert barrier (gap). The shock sensitivity of the test material is characterized by the gap thickness for which the probability of detonation is 0.5.

Hercules Inc. is using the Naval Ordnance Laboratory (NOL)<sup>\*</sup> large-scale gap test<sup>1</sup> as a means of evaluating the effects of rocket propellant formulation and processing variables on the reaction of the propellant to shock. The Los Alamos Scientific Laboratory (LASL) has used its own version of the gap test for many years, primarily as a measure of the hazards associated with explosive materials.<sup>2</sup> Here we model these tests numerically to provide a better understanding of the details of the processes involved.

---

\*NOL, White Oak, is now Naval Surface Weapons Center, Silver Spring, Maryland.

## II. EXPERIMENT AND MODEL

The experimental arrangement of the LASL standard, or large-scale, gap test is shown in Fig. 1.<sup>2</sup> The Dural spacer and relatively long booster are used to obtain greater precision in the tests. The gap length at which detonation of 50% of the samples would be expected to occur is estimated by the up-and-down procedure. A 0.25-mm step height is used for the final determination of the 50% point.

The NOL large-scale gap test is shown in Fig. 2. A J-2 blasting cap (Hercules) is used to initiate the standard donor, which is two pressed pentolite pellets with density of 1.56 g/cm<sup>3</sup>. The gap is made of Plexiglas (polymethyl methacrylate) disks and cellulose acetate cards. The test explosive is formed to fit a seamless steel tube with a 5.6-mm-thick wall. A 9.5-mm-thick mild steel witness plate is used. A "go" result is defined by a clean hole punched in the plate. The test procedure is a modification of the Bruceton up-and-down technique.

The computation of gap test behavior was performed with the two-dimensional reactive hydrodynamic code 2DE<sup>3,4</sup> using the Forest Fire burn rate<sup>3,5</sup> for all the explosives and propellants except pentolite. Because Pop plot data are not available to derive Forest Fire parameters for pentolite, the C-J volume burn model<sup>3</sup> was used for this explosive. The equation-of-state data used in these calculations are given in Appendix A. The Forest Fire burn rate parameters, Pop plot

data, and C-J volume burn parameters are given in Appendix B. The Plexiglas was modeled with elastic-plastic flow, with shear modulus = 1.5 GPa and yield strength = 0.5 GPa.

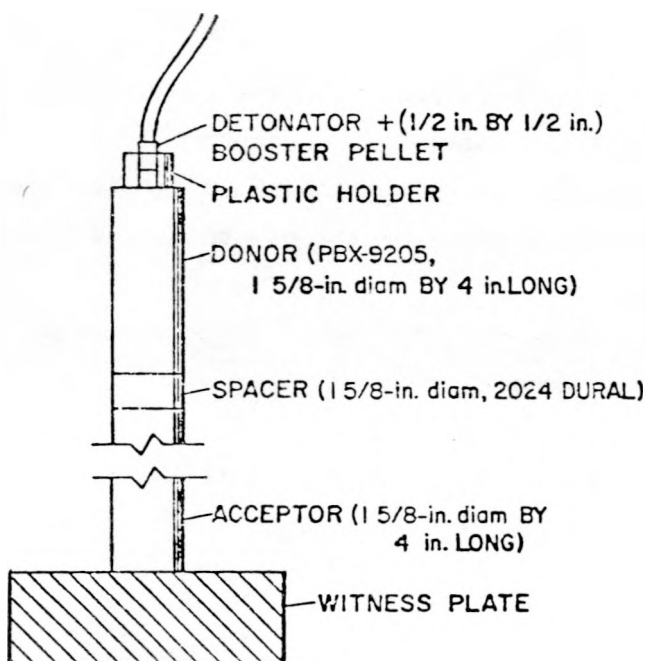


Fig. 1.  
LASL standard gap test assembly.

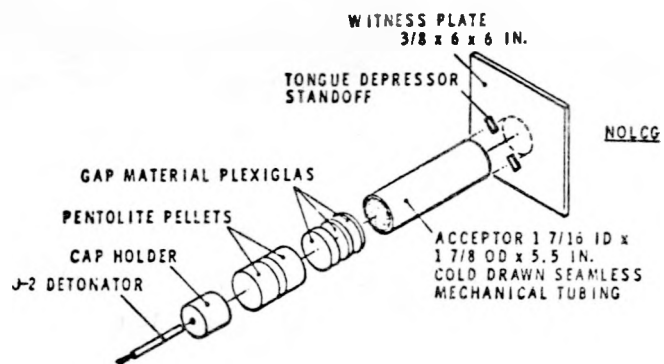


Fig. 2.  
NOL large-scale gap test configuration.

The gap tests were modeled at their true dimensions, using a 2.064-mm cell for the LASL test and a 1.826-mm cell for the NOL test. The model geometries are shown in Figs. 3 and 4. Unconfined NOL gap test calculations were made with the same model, with the steel tube replaced by air. The LASL test was initiated by a full-radius hot spot to model the effect of the 1/2-in. tetryl booster pellet. The NOL test was initiated by a hot spot of 3.7-mm radius and length to model the

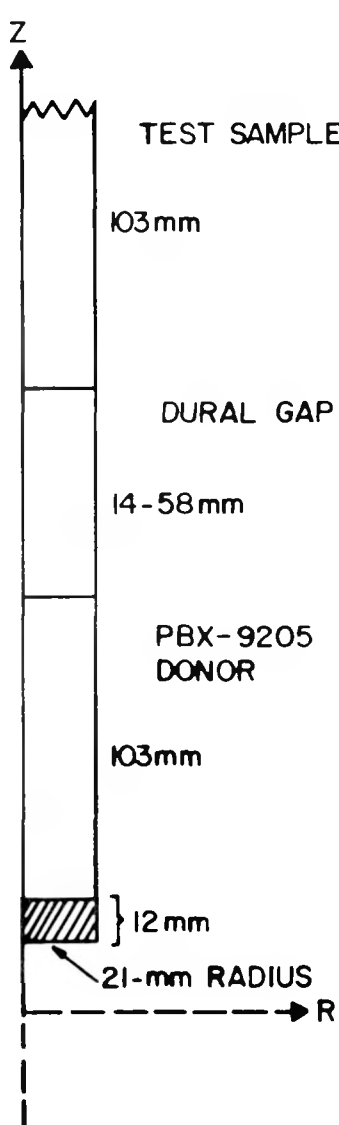


Fig. 3.

LASL gap test model. The symmetry axis of the cylindrical assembly is at the left. The initiation of the donor is modeled by a 21-mm-radius, 12-mm-long hot spot.

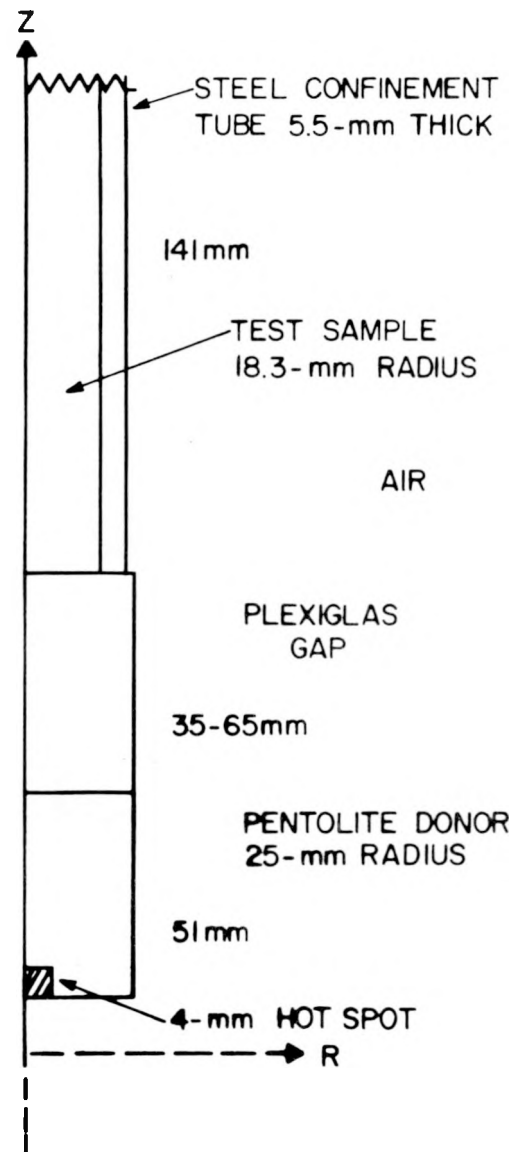


Fig. 4.

NOL gap test model. The initiation of the donor is modeled by a hot spot of 3.7-mm radius and length.

effect of the J-2 cap used by Hercules Inc. The hot spot is fully reacted explosive (gaseous products) with density and energy initialized to isentrope conditions at  $\sim 1.02 \times C-J$  pressure.

### III. RESULTS AND DISCUSSION

The detonation behavior of the donor cylinders is shown in Figs. 5 and 6 by a series of contour plots of mass fraction and density. The mass fraction  $W$  is defined such that  $W = 1$  for a solid and  $W = 0$  for a gas, with a continuous variation between these limits for a burning explosive. The nearly planar detonation wave in the PBX-9205 donor of the LASL test runs steady at 28 GPa. This agrees

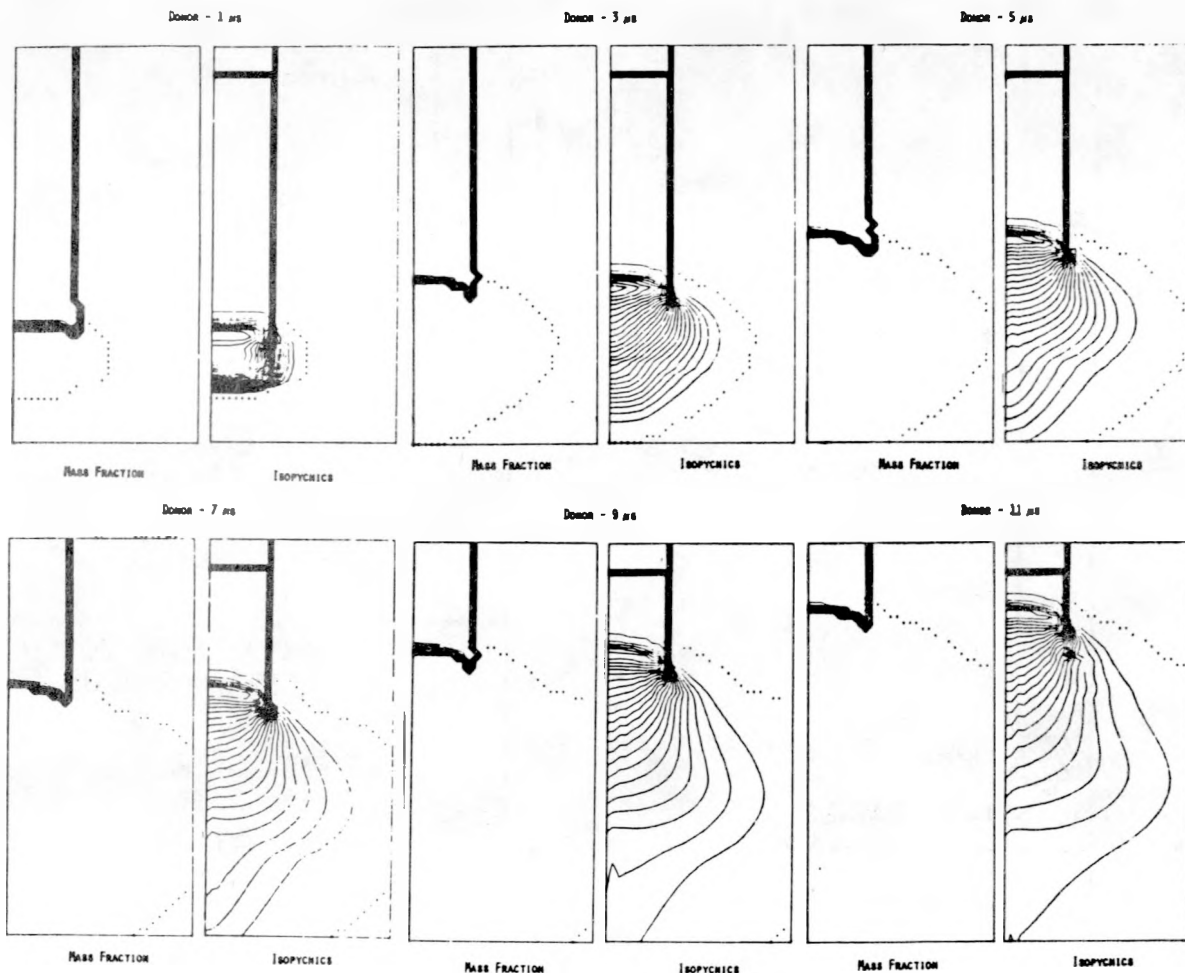


Fig. 5.

Detonation of the LASL gap test donor. PBX-9205 cylinder, 21-mm radius by 102 mm long, at 1, 3, 5, 7, 9, and 11  $\mu$ s. Contour plots of mass fraction (0.05 interval) and density (0.1-g/cm<sup>3</sup> interval).

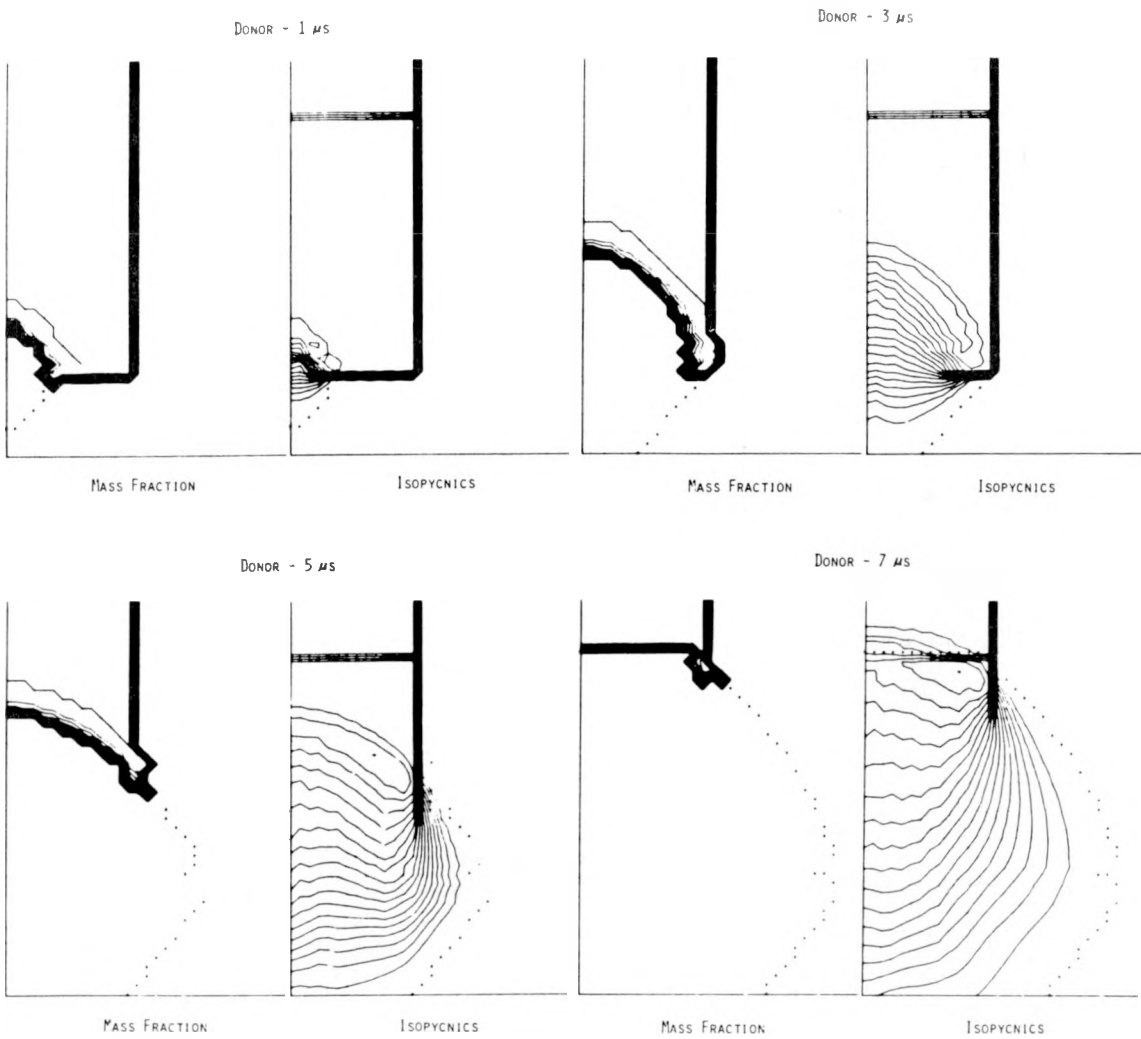


Fig. 6.

Detonation of the NOL gap test donor. Pentolite cylinder, 25-mm radius by 51 mm long, at 1, 3, 5, and 7  $\mu$ s. Contour plots of mass fraction (0.05 interval) and density ( $0.1\text{-g/cm}^3$  interval). The shock has entered the Plexiglas gap at 7  $\mu$ s.

well with the C-J pressure of 28.1 GPa obtained from a BKW calculation.<sup>6</sup> This donor was also modeled with a 12.4-mm-diam hot spot initiation, which ran to the same steady-state pressure. The strongly divergent detonation wave in the pentolite donor of the NOL test reaches a steady pressure of 14.5 GPa, which is much less than the C-J pressure of 22.8 GPa.<sup>6</sup> The particle velocity ( $U_p$ ) at the detonation front was 1.15 mm/ $\mu$ s and the detonation velocity was 7.5 mm/ $\mu$ s.

The initial shock pressure in the gap is obtained graphically as the intersection of the isentrope\* of the donor detonation products with the Hugoniot of the gap material. These curves are shown in the pressure-particle velocity plane in Fig. 7. The intersection points, shown as squares, give induced pressures of 33.5 GPa for the LASL test and 10.3 GPa for the NOL test. The isentropes, calculated by BKW,<sup>6</sup> are run through the C-J point for PBX-9205 and through the point ( $p = 14.5$ ,  $U_p = 1.15$ ) obtained from these calculations for pentolite. These reference points are indicated as circles in Fig. 7. The peak pressures that are developed in the gap material by the passage of the shock wave are readily obtained from these calculations. This permits the construction of calibration curves of gap pressure vs gap thickness (Figs. 8 and 9). The NOL test has been calibrated experimentally,<sup>7</sup> and the resulting curve is also shown in Fig. 9. The high pressures at small gap (<10 mm) are not experimental values, but are based on a zero gap value derived from the graphical matching described above, using the assumption of C-J pressure in the pentolite.\*\* The experimental and calculated curves agree within their uncertainties for gap thicknesses > 10 mm. The

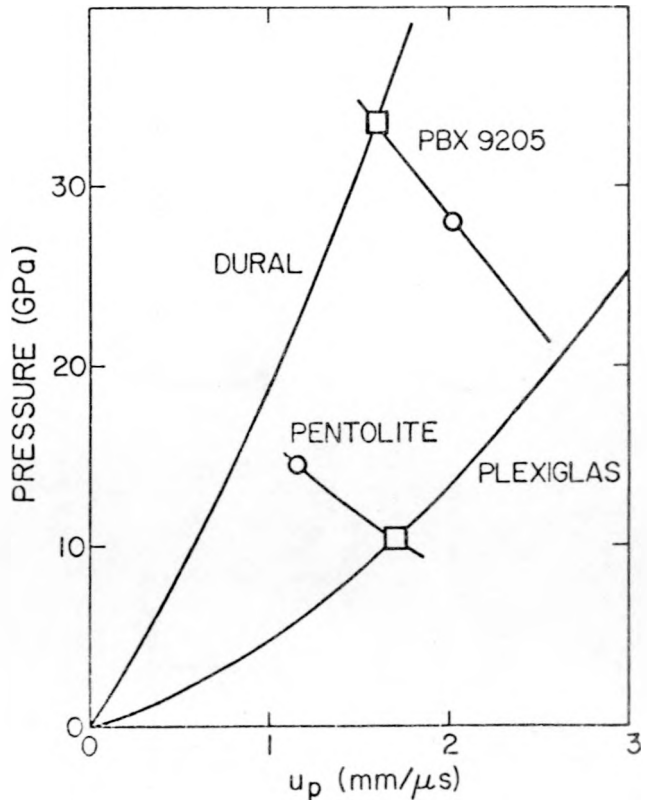


Fig. 7.  
Impedance match at donor-gap interface. The intersection of the isentrope through the detonation state (pressure-particle velocity) with the Hugoniot of the gap material defines the initial pressure in the gap.

\*Because the matching point for the PBX-9205/Dural is above the C-J point, the correct curve to be used is the detonation products shock Hugoniot. This is approximated by an extrapolation of the BKW isentrope beyond the C-J point.

\*\*This assumption is not correct. It has been shown from theoretical arguments that the Rankine-Hugoniot equations and the Chapman-Jouguet condition are not appropriate to the description of a "steady" diverging cylindrical or spherical detonation wave.<sup>8</sup> Taylor also concluded from simpler considerations that the C-J pressure may not be attained although the C-J detonation velocity will be realized in a spherical wave.<sup>9</sup> This position is also supported by experiment (Ref. 2, pp. 116-221).

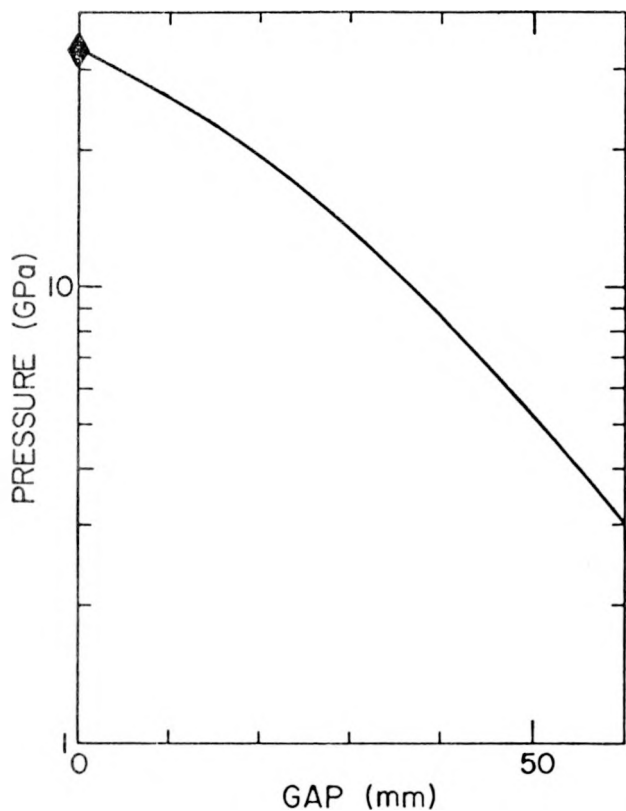


Fig. 8.

LASL standard gap test. Shock pressure in the Dural gap.

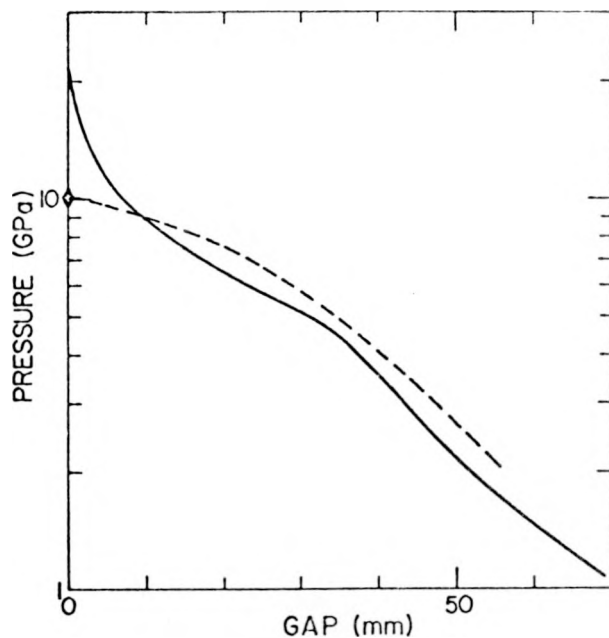


Fig. 9.

NOL large-scale gap test. Shock pressure in the Plexiglas gap. The solid curve is from an experimental calibration for gap lengths  $> 10$  mm (Ref. 7). The dashed curve is from this study.

calculated curve will be used for all further discussion. There is no experimental calibration of the LASL test.

To test our model at both ends of the normal sensitivity range, the LASL standard gap test was run with TATB and PBX-9404 as test explosives. The results of these calculations are summarized in Table I. The pressure in the Dural gap when the shock wave hits the test sample ( $P_g$ ) is taken from the calculated calibration curve (Fig. 8). The pressure induced in the sample ( $P_i$ ) by this shock is obtained from a graphical impedance match, as shown in Fig. 10 for PBX-9404. The calculated  $P_i$  is estimated from the early shock peaks in the test sample with an uncertainty of  $\sim 5\%$ . The difference between the two values of  $P_i$  is due entirely to the effect of shock-induced chemical reaction in the explosive. This was confirmed by performing the calculation with nonreactive samples (same material, but with no chemical reaction permitted). The values of  $P_i$  obtained in this manner were 15.6 GPa in TATB at 14.4 mm and 2.5 GPa in PBX-9404 at 51.6 mm. These results are in quantitative agreement with the impedance match values of 16.3 and

TABLE I  
LASL STANDARD GAP TEST

Gap (mm)	TATB		PBX-9404			
	14.4	20.6	43.3	47.5	51.6	55.7
Pressures (GPa)						
Dural gap <sup>a</sup>	23.2	19.0	7.3	5.9	4.8	3.8
Induced in sample:						
Calculation	23.5	13.5	8.0	4.0	3.0	2.4
Impedance match	16.3	13.0	4.2	3.3	2.6	2.0
Run distance (mm)						
Pop plot	3	6	5	7	9	13
Calculation	7	--	4	8	19	--
Experimental 50% gap (mm)	21.9 <sup>b</sup>		51.9 - 57.6 <sup>c</sup>			

<sup>a</sup>Pressures from the calibration curve, Fig. 8.

<sup>b</sup>Experimental sample had  $\rho = 1.870$ ; calculation based on limited Pop plot data for material with  $\rho = 1.876$ .

<sup>c</sup>This range includes all separate observations for PBX-9404 with  $\rho > 1.84$  (Ref. 2). Calculation based on  $\rho = 1.844$ .

2.6 GPa. The detonation of TATB at a 14.4-mm gap is shown in Fig. 11 with a series of mass fraction contour plots. The shock wave enters the sample between 15 and 16  $\mu$ s after the start of the calculation, and leads immediately to significant reaction, shown by the growing dark area at 16 and 17  $\mu$ s. The region of complete reaction that appears at 18  $\mu$ s (white area surrounded by the zone of partial reaction) signals the transition to a detonation, which proceeds in the final two frames. The length of run to detonation is determined from these plots with an uncertainty of  $\sim 1$  mm. The detonation of PBX-9404 at a 51.6-mm gap is shown in Fig. 12 with a similar series of plots. The shock wave enters the sample between 21 and 22  $\mu$ s, but at the much lower pressure the reaction proceeds more slowly, and the transition to detonation is not observed until 29  $\mu$ s from zero time. The sharp curvature of the shock front is seen from the isopycnic contour plots of Fig. 13. This series starts with the entry of the shock wave, rather than with the first observable reaction of Fig. 12, and proceeds only to the detonation point at 29  $\mu$ s.

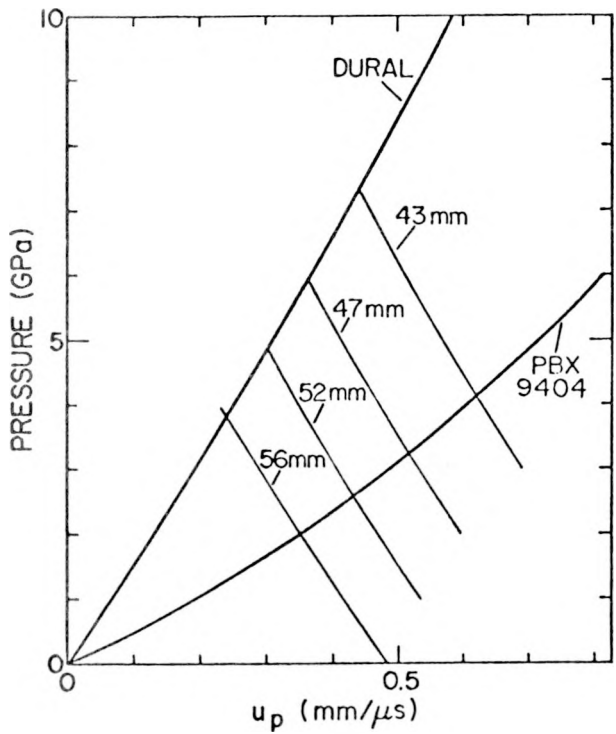


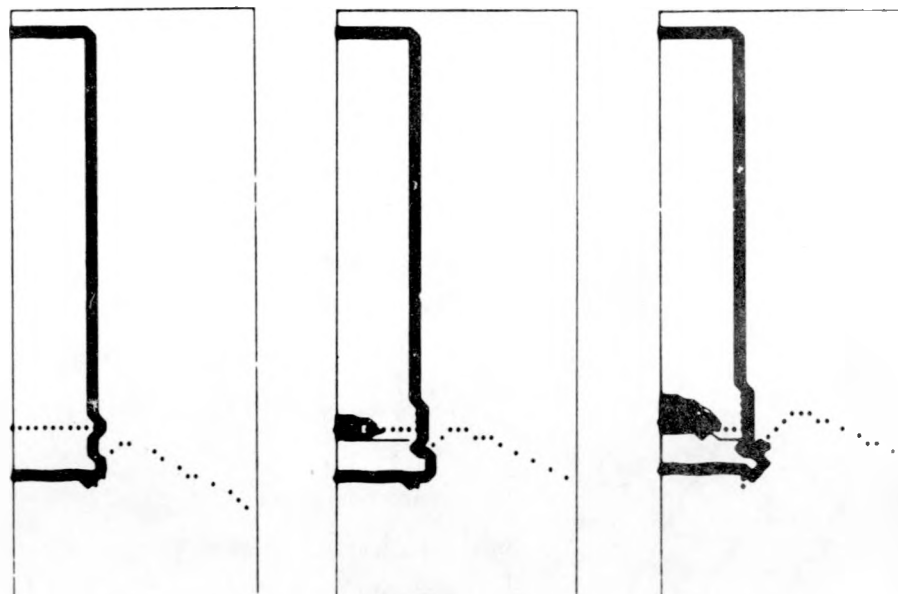
Fig. 10.

LASL gap test. Impedance match at the gap-test sample interface for PBX-9404. The Dural Hugoniot is reflected through the pressure determined from Fig. 8 for a given gap length. The intersection of the reflected Hugoniot with the PBX-9404 Hugoniot defines the shock pressure induced in the test sample.

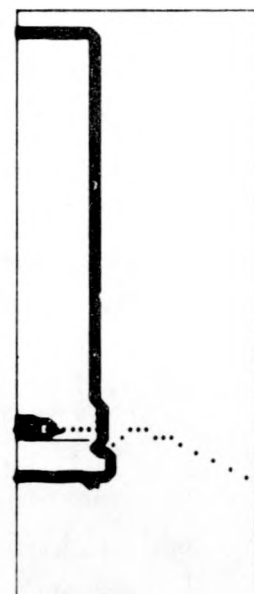
Pop plot is determined. It is also apparent from the data in Table I that the critical gap length is not related to a constant value of  $\chi^*$ .

The NOL large-scale gap test was run with VTQ-2 and Composition B as test explosives. The VTQ-2 was also run without the steel tube to study the effect of confinement. The results of these calculations are summarized in Table II. The values of  $P_g$  and  $P_i$  were determined in the same manner as those for the LASL gap test. A nonreactive calculation with VTQ-2 gave  $P_i = 5.2$  GPa at a 40.2-mm gap, in excellent agreement with the value of 5.3 GPa obtained from the impedance match. The detonation of VTQ-2 at a 40.2-mm gap is shown in Fig. 15 with a series of mass fraction contour plots. The shock wave enters the sample between 16 and 17  $\mu$ s after the start of the run. Significant reaction is observed at 18  $\mu$ s, and the partially reacted zone spreads behind the shock front, with detonation observed

The expected length of run to detonation ( $\chi^*$ ) in the test sample is determined from the Pop plot using the value of  $P_i$  obtained from the impedance matching. The Pop plots used in this work are shown in Fig. 14, and their equations are given in Appendix B. The actual  $\chi^*$  obtained from these calculations is found to be significantly longer than the expected value for gap lengths near the critical point (the maximum gap length for which detonation is observed). The data in Table I show that the ratio  $\chi^*(\text{calc.})/\chi^*(\text{Pop plot})$  reaches a value of approximately two near the critical gap length. The data for PBX-9404 indicate that this ratio drops to one for shorter gap lengths. This difference is attributed to the nonplanar nature of the shock wave entering the test sample (Fig. 13). This is in contrast with the plane-wave, one-dimensional wedge shots from which the



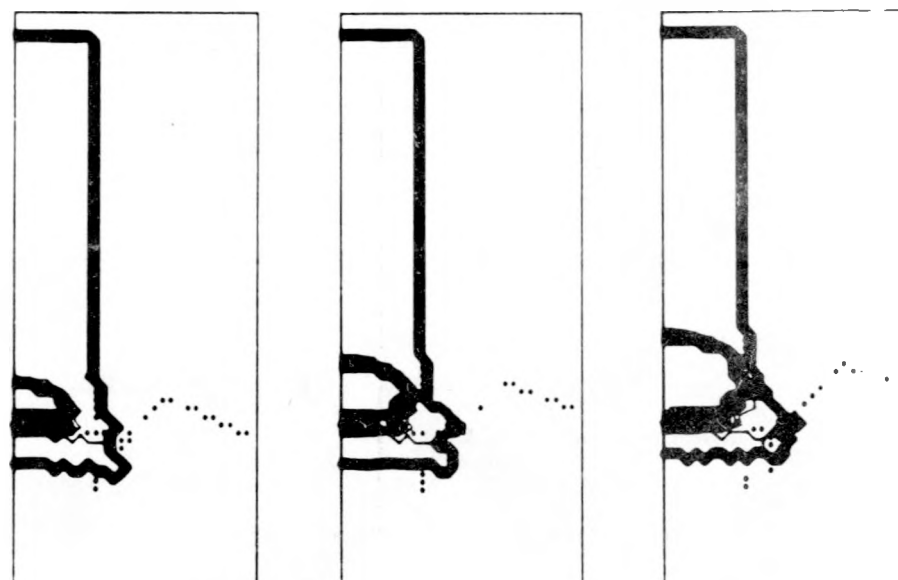
15  $\mu$ s



16  $\mu$ s



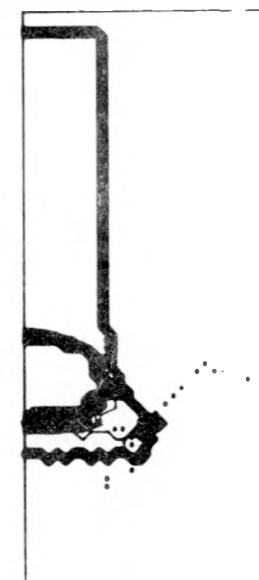
17  $\mu$ s



18  $\mu$ s



19  $\mu$ s



20  $\mu$ s

Fig. 11.

LASL gap test. Detonation of TATB at a 14.4-mm gap. Mass fraction contour plots.

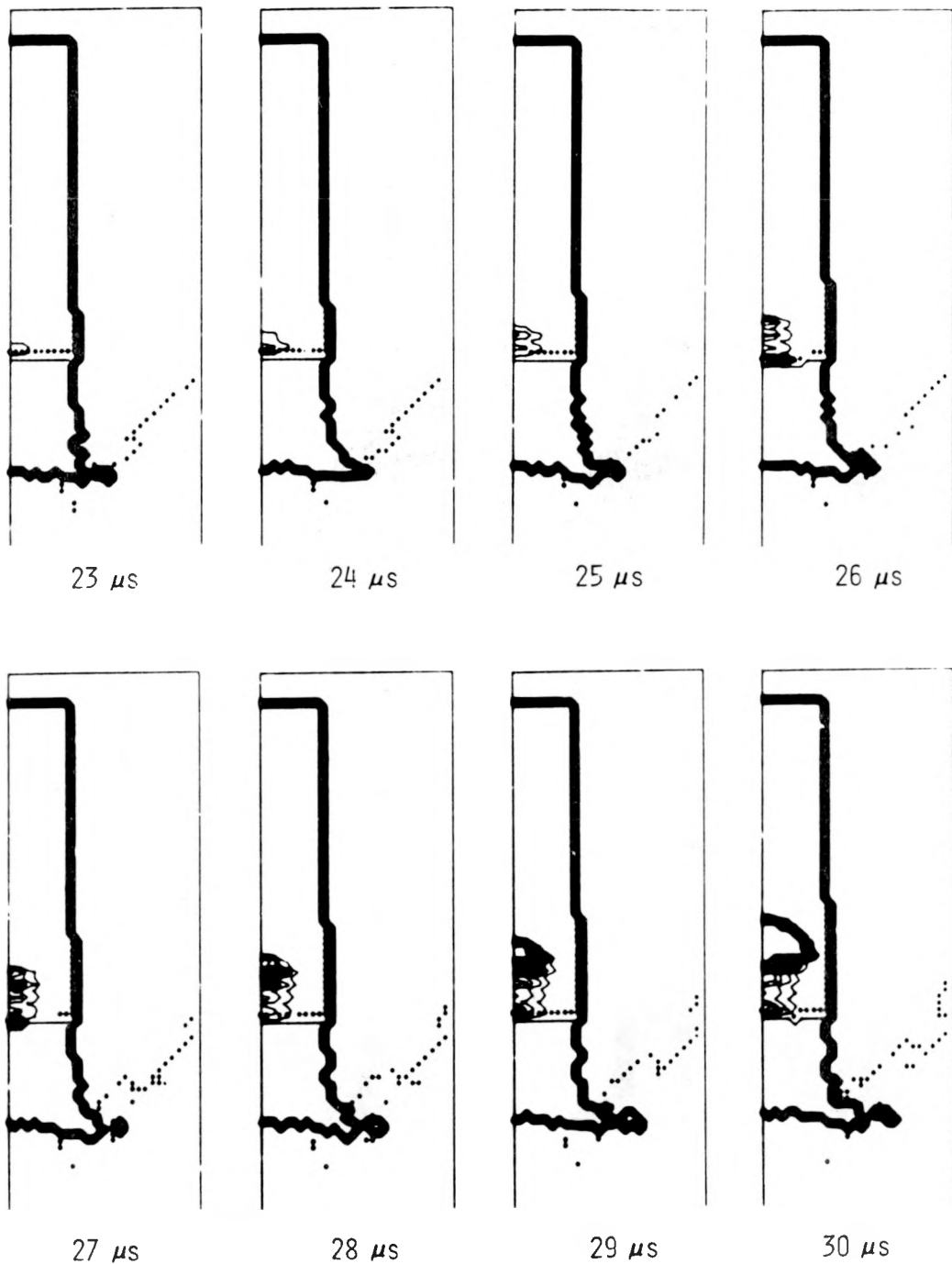
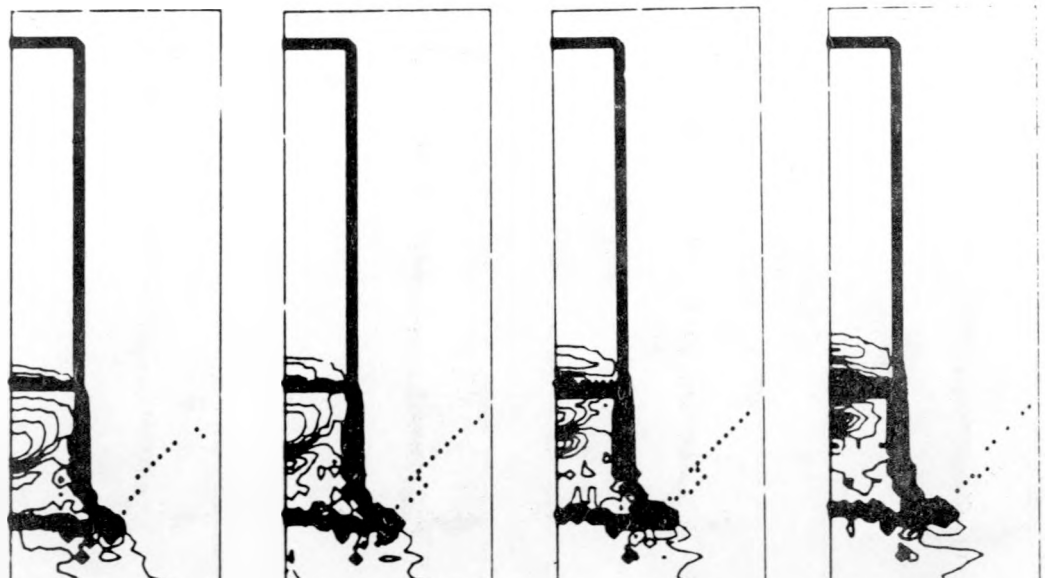


Fig. 12.  
LASL gap test. Detonation of PBX-9404 at a 51.6-mm gap. Mass fraction contour plots.

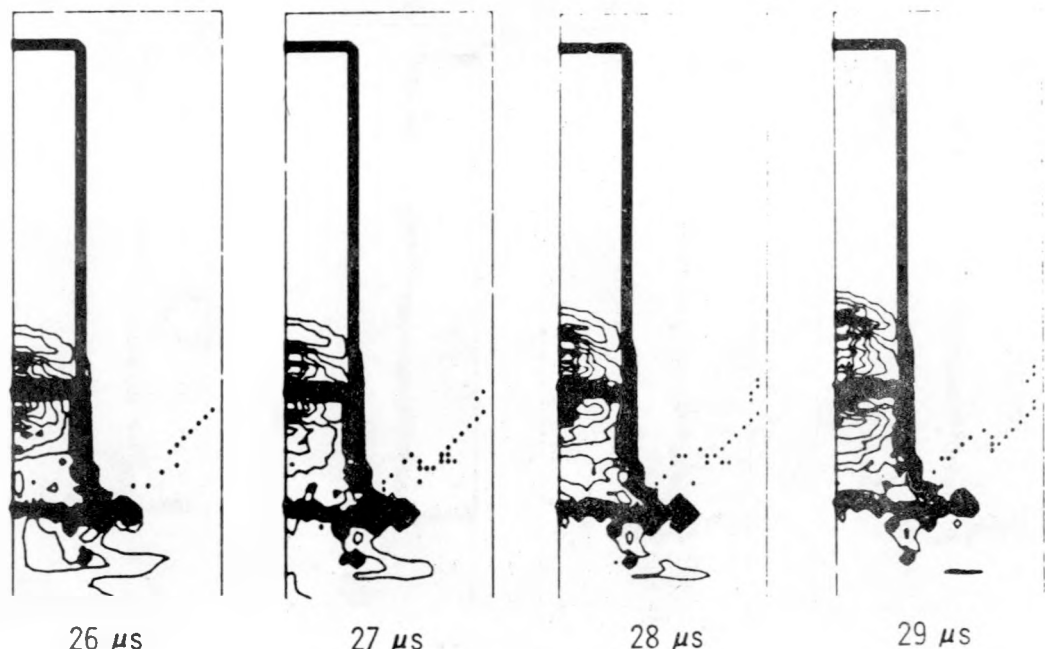


22  $\mu$ s

23  $\mu$ s

24  $\mu$ s

25  $\mu$ s



26  $\mu$ s

27  $\mu$ s

28  $\mu$ s

29  $\mu$ s

Fig. 13.

LASL gap test. Shock wave in PBX-9404 at a 51.6-mm gap. Isopycnic contour plots ( $0.1\text{-g/cm}^3$  interval).

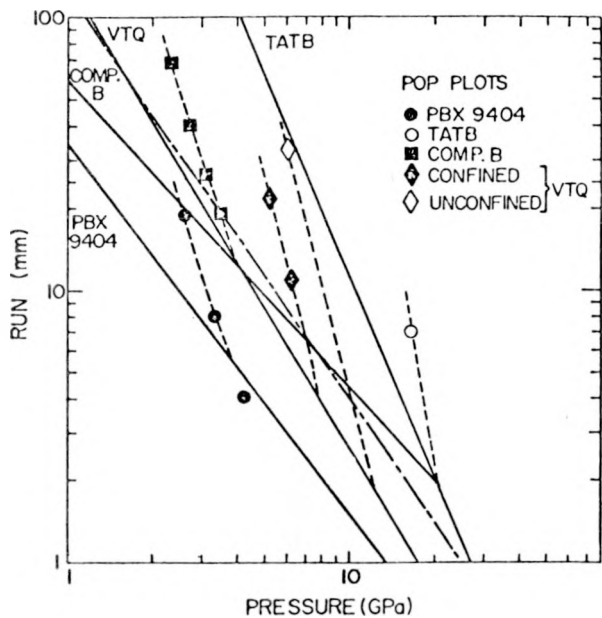


Fig. 14.

Pop plots of the test materials of this study, shown by solid lines. An alternate Pop plot for Composition B is shown by the dashed (—) line, indicating the degree of uncertainty in this material. The run-pressure points obtained from this study are plotted with dotted lines to indicate approximate two-dimensional "Pop plots" defined by the gap tests.

at 25  $\mu$ s. The general behavior of the shock wave is shown by isopycnic contour plots in Fig. 16. The shock front is curved when it enters the sample at  $\sim$ 17  $\mu$ s, and is significantly stronger on the axis. This is changed by the steel confinement tube, and by 20  $\mu$ s the built-up shock wave is stronger at the tube wall, leading to detonation at the wall instead of in the center. The detonation of VTQ-2 at a 36.5-mm gap without the steel confinement tube is shown in Figs. 17 and 18. In the absence of the supporting tube wall the curvature of the shock front increases, giving a limited zone of partial reaction and leading to detonation in the center of the sample at 26  $\mu$ s. The ratio  $\chi^*(\text{calc.})/\chi^*(\text{Pop plot})$  is greater for the NOL gap test than for the LASL test. This may be a consequence of the more sharply curved shock front in the NOL test.

#### IV. CONCLUSIONS

We have modeled successfully the LASL and NOL large-scale (standard) gap tests using the 2DE reactive hydrodynamic code with Forest Fire burn rates. The results of the calculations agree well with the experimental values. The worst agreement was obtained with Composition B, which may be a consequence of the Pop plot that was used. The two available Pop plots for Composition B are shown in Fig. 14. The lower, more sensitive curve was used for these calculations. The upper curve would give a shorter critical gap length, probably less than the experimental value.

The calibration of peak pressure in the gap ( $P_g$ ) vs gap length ( $\chi$ ) was obtained from these calculations. The calculated curve for the NOL gap test agrees

TABLE II  
NOL LARGE-SCALE GAP TEST

	VTQ-2			Composition B				
Gap (mm) (in.)	36.5 1.44	40.2 1.58	43.8 1.73	47.5 1.87	51.1 2.01	54.8 2.16	58.4 2.30	62.1 2.44
Pressures (GPa)								
Plexiglas gap <sup>a</sup>	4.7	4.0	3.4	2.9	2.5	2.2	1.9	1.6
Induced in sample:								
Calculation	8.0	6.5	5.3	4.5	3.8	3.3	2.7	2.3
Impedance match	6.1	5.2	4.3	3.5	3.1	2.7	2.3	1.9
Run distance (mm)								
Pop plot	6	8	11	15	17	20	24	29
Calculation	11	22	--	19	27	40	69	--
Transit time (μs)	24	26						
Experimental 50% gap (in.)			1.60				2.01 - 2.18	
No confinement								
Run distance (calc.)	33	--						
Experimental 50% gap			1.50					

<sup>a</sup>Pressures from the calibration curve, Fig. 9.

with the published experimental curve<sup>7</sup> for  $x > 10$  mm, and is much better for shorter gap lengths. These results provide the first calibration curve for the LASL test.

The distances of run to detonation obtained from these calculations are plotted vs the induced pressures ( $P_i$ ) in Fig. 14 for comparison with the Pop plots obtained from wedge tests. The run distances from the gap tests are significantly longer than those from the wedge tests at induced pressures near the gap length, but they approach each other at higher pressures. The critical run distance, i.e., the observed run distance at the critical gap length, clearly increases with increasing gap length in both types of gap tests. It is also clear from this study that the NOL gap test should always register a shorter critical gap length when the test sample is not confined.

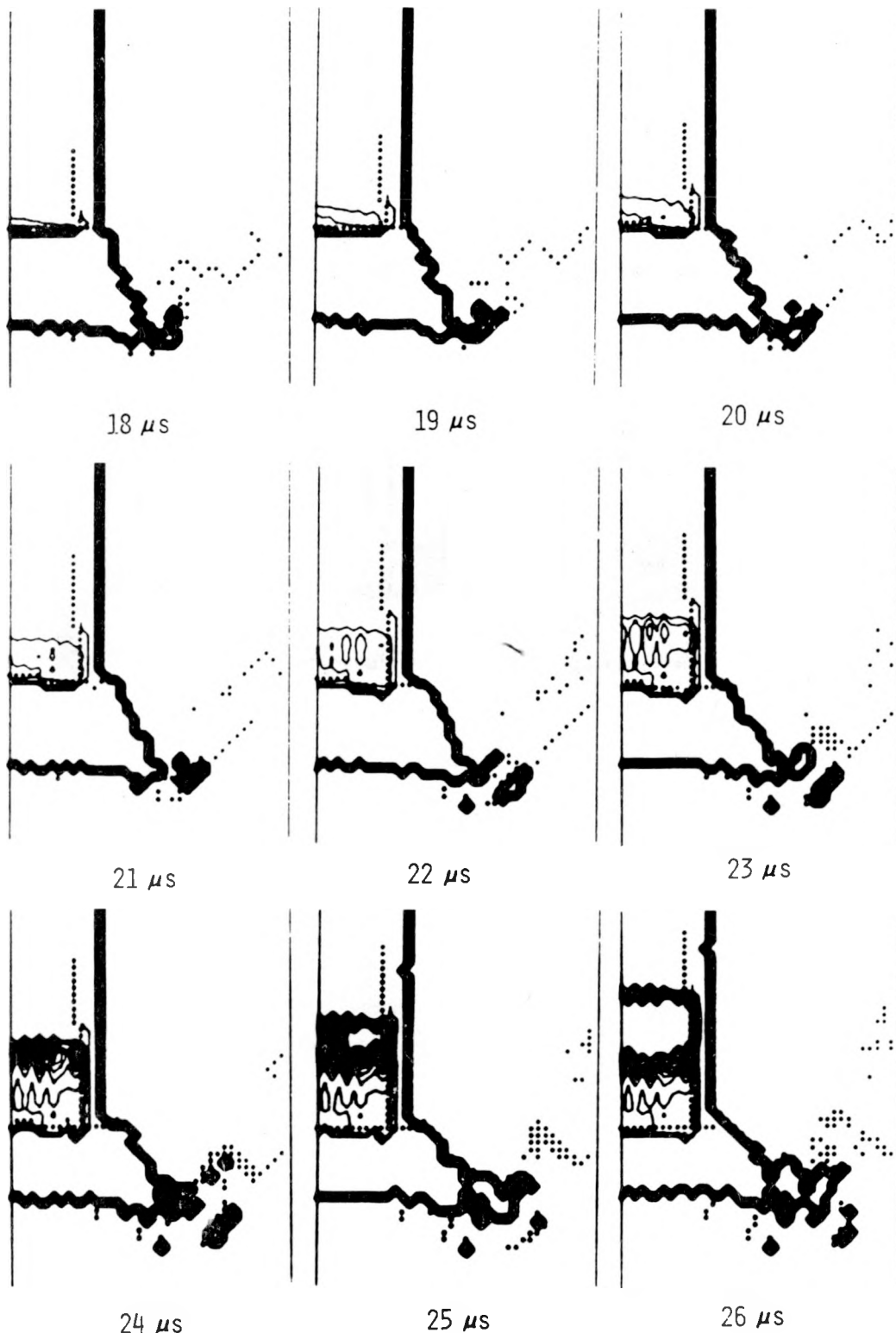


Fig. 15.

NOL gap test. Detonation of VTQ-2 at a 40.2-mm gap. Mass fraction contour plots.

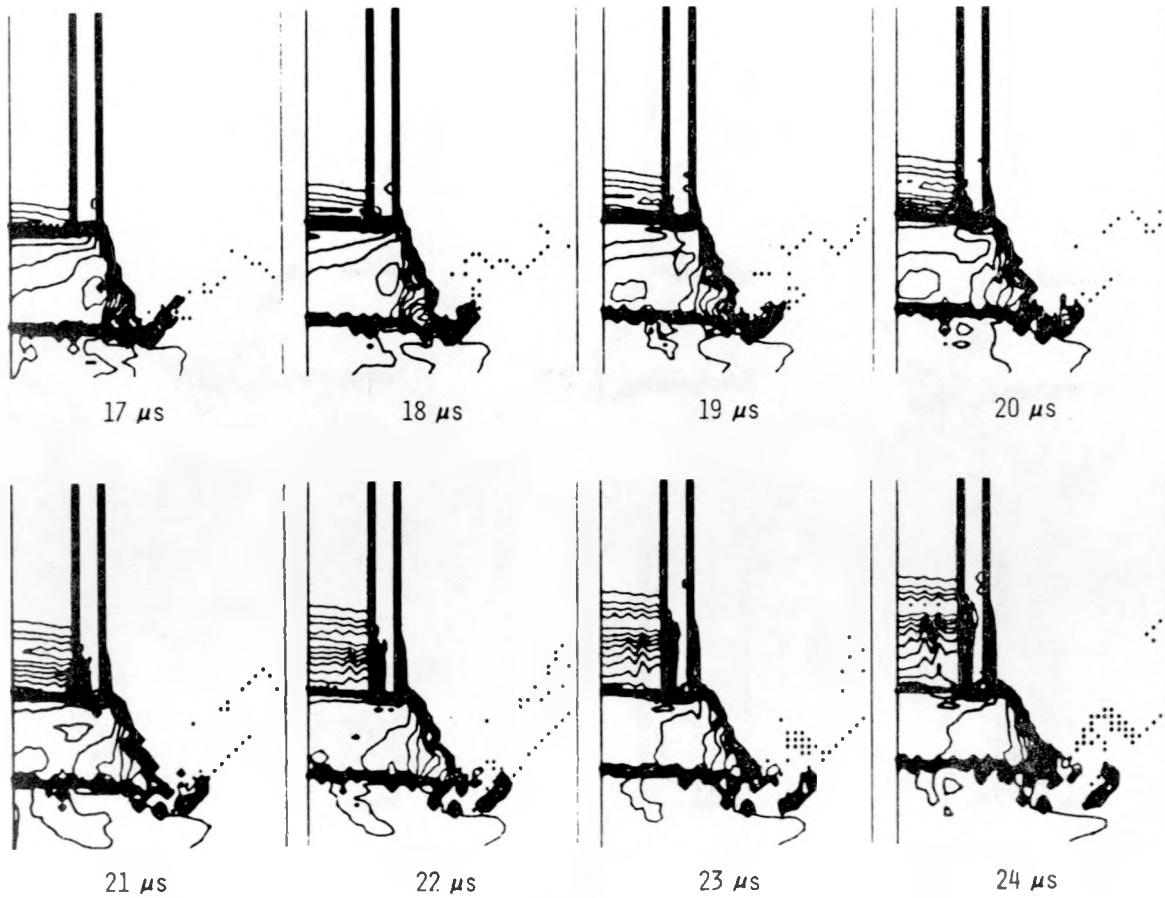


Fig. 16.

NOL gap test. Shock wave in VTQ-2 at a 40.2-mm gap. Isopycnic contour plots (0.1-g/cm<sup>3</sup> interval).

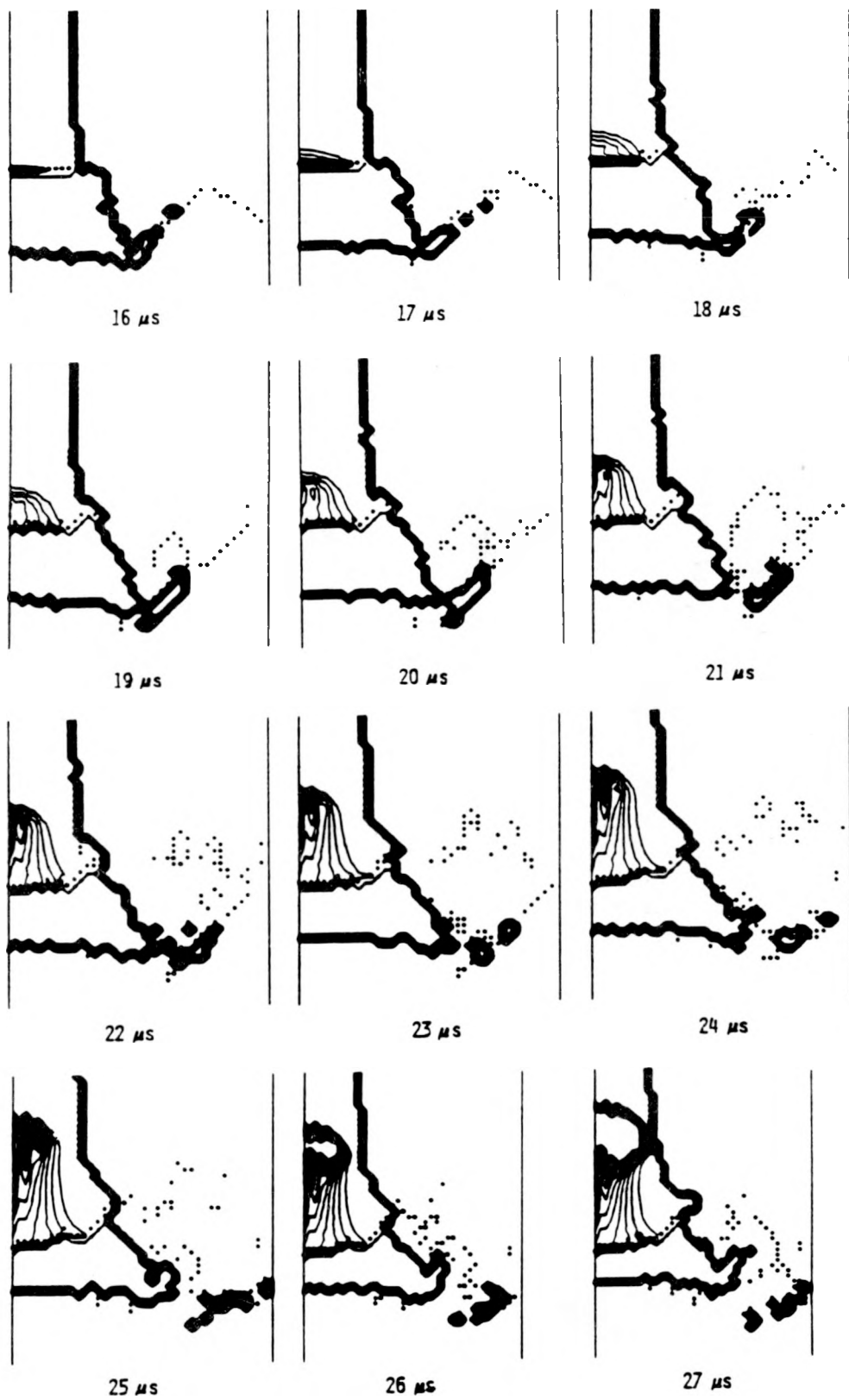


Fig. 17.

NOL gap test without the steel confinement tube. Detonation of VTQ-2 at a 36.5-mm gap. Mass fraction contour plots.

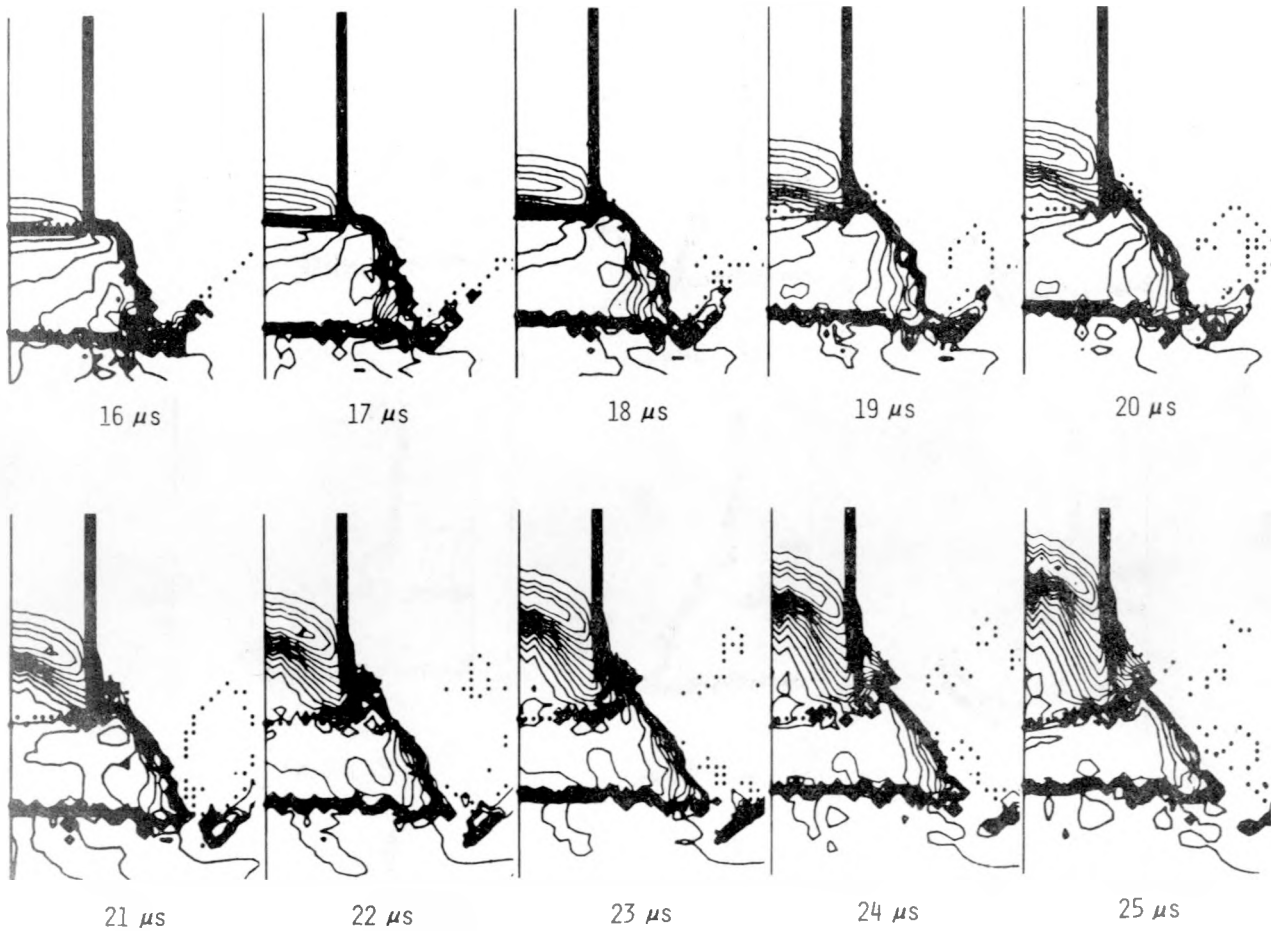


Fig. 18.

NOL gap test without the steel confinement tube. Shock wave in VTQ-2 at a 36.5-mm gap. Isopycnic contour plots ( $0.1\text{-g}/\text{cm}^3$  interval).

## APPENDIX A

### EQUATION OF STATE

The HOM equation of state is used to solve for pressure P and temperature T in a cell, with specific volume V and specific internal energy I as input. The shock velocity  $U_s$  and the particle velocity  $U_p$  are related by

$$U_s = C + S U_p .$$

The equations for a solid are

$$P_H = C^2 (V_0 - V) / [V_0 - S(V_0 - V)]^2$$

$$X = \ln V$$

$$\ln T_H = F + G X + H X^2 + I X^3 + J X^4$$

$$I_H = (1/2) P_H (V_0 - V)$$

$$P = (\gamma/V)(I - I_H) + P_H$$

$$T = (I - I_H)(23 890)/C_V + T_H .$$

The equations for a gas are

$$X = \ln V$$

$$Y = \ln P_i$$

$$Y = A + B X + C X^2 + D X^3 + E X^4$$

$$\ln I_i = K + L Y + M Y^2 + N Y^3 + O Y^4$$

$$I_i = I_i - Z$$

$$\ln T_i = Q + R X + S X^2 + T X^3 + U X^4$$

$$-1/\beta = R + 2 S X + 3 T X^2 + 4 U X^3$$

$$P = [1/(\beta V)](I - I_i) + P_i$$

$$T = (I - I_i)(23 890)/C'_V + T_i .$$

The solution for a cell with more than one component is based on combinations of these equations.<sup>3,4</sup>

The equation-of-state parameters used in this study are tabulated in Table A-I. The units are volume ( $\text{cm}^3/\text{g}$ ), energy ( $\text{Mbar}\cdot\text{cm}^3/\text{g}$ ), pressure ( $\text{Mbar}$ ), temperature (K), velocity ( $\text{cm}/\mu\text{s}$ ), and heat capacity ( $\text{cal}/\text{g}\cdot\text{K}$ ).

TABLE A-I  
EQUATION-OF-STATE PARAMETERS

<u>Dural</u>	
C	$5.35000000000000\text{E-}01$
S	$1.35000000000000\text{E+}00$
F	$-2.07547507908\text{E+}01$
G	$-1.15617830366\text{E+}02$
H	$-1.77762573069\text{E+}02$
I	$-1.14252754176\text{E+}02$
<u>Plexiglas</u>	
C	$2.43200000000000\text{E-}01$
S	$1.57850000000000\text{E+}00$
F	$5.29380243506\text{E+}00$
G	$-4.24950371368\text{E+}00$
H	$-1.55055576332\text{E+}01$
I	$-3.08638075572\text{E+}01$
<u>Steel</u>	
C	$4.58000000000000\text{E-}01$
S	$1.51000000000000\text{E+}00$
F	$-3.82382587453\text{E+}03$
G	$-7.03211954024\text{E+}03$
H	$-4.82670213890\text{E+}03$
I	$-1.46678402118\text{E+}03$
<u>Air</u>	
A	$-4.50602542688\text{E+}00$
B	$-1.27546110628\text{E+}00$
C	$-3.74276600292\text{E-}03$
D	$1.23929236747\text{E-}02$
E	$-2.07694122929\text{E-}03$
K	$-1.62655447438\text{E+}00$
L	$9.05283146618\text{E-}02$
M	$2.69004997726\text{E-}03$
N	$-5.43583122192\text{E-}05$
O	$-1.58521895338\text{E-}06$
Q	$8.22644581441\text{E+}00$
R	$-2.51525130950\text{E-}01$
S	$-1.34446940047\text{E-}02$
T	$1.40871016422\text{E-}02$
U	$-2.18132189985\text{E-}03$
C'	$5.00000000000\text{E-}01$
Z	$1.00000000000\text{E-}01$

TABLE A-I (cont)

PBX-9205

C	2.40000000000E-01	D	3.35495910100E-02
S	2.05000000000E+00	E	-1.46326377300E-02
F	-2.41732675010E+01	K	-1.55974151000E+00
G	-1.39872107139E+02	L	5.26416845600E-01
H	-2.37879021477E+02	M	8.05520662000E-02
I	-1.70729283235E+02	N	6.44578515600E-03
J	-4.16327143692E+01	O	2.11631338000E-04
Y	1.50000000000E+00	Q	7.42577438000E+00
C <sub>V</sub>	3.00000000000E-01	R	-4.65906433000E-01
V <sub>0</sub>	5.91715976000E-01	S	4.08137430000E-02
$\alpha$	5.00000000000E-05	T	2.46604860000E-02
A	-3.52962204200E+00	U	-7.77029500000E-03
B	-2.56501757700E+00	C <sub>V</sub>	5.00000000000E-01
C	2.56358164700E-01	Z	1.00000000000E-01

PBX-9404

C	2.42300000000E-01	D	1.39083578508E-02
S	1.88300000000E+00	E	-1.13963024075E-02
F	-9.04187222042E+00	K	-1.61913041133E+00
G	-7.13185252435E+01	L	5.21518534192E-01
H	-1.25204979360E+02	M	6.77506594107E-02
I	-9.20424177603E+01	N	4.26524264691E-03
J	-2.21893825727E+01	O	1.04679999902E-04
Y	6.75000000000E-01	Q	7.36422919790E+00
C <sub>V</sub>	4.00000000000E-01	R	-4.93658222389E-01
V <sub>0</sub>	5.42299349241E-01	S	2.92353060961E-02
$\alpha$	5.00000000000E-05	T	3.30277402219E-02
A	-3.53906259964E+00	U	-1.14532498206E-02
B	-2.57737590393E+00	C <sub>V</sub>	5.00000000000E-01
C	2.60075423332E-01	Z	1.00000000000E-01

TATB

C	2.00000000000E-01	D	7.17142061164E-02
S	2.05000000000E+00	E	-3.02093547088E-02
F	-1.21280271935E+01	K	-1.58230649189E+00
G	-8.11672546025E+01	L	5.41924059120E-01
H	-1.31649312523E+02	M	9.72221045331E-02
I	-8.63814452915E+01	N	8.81767684503E-03
J	-1.68899480903E+01	O	3.20478862732E-04
Y	1.50000000000E+00	Q	7.15134298485E+00
C <sub>V</sub>	3.00000000000E-01	R	-5.17846629749E-01
V <sub>0</sub>	5.33049040512E-01	S	5.71251032056E-02
$\alpha$	5.00000000000E-05	T	6.57471769211E-03
A	-3.83981823690E+00	U	-6.57292774182E-03
B	-2.65390199257E+00	C <sub>V</sub>	5.00000000000E-01
C	2.39445476232E-01	Z	1.00000000000E-01

TABLE A-I (cont)

Pentolite

C	2.71500000000E-01	D	3.30073305731E-02
S	2.57600000000E+00	E	-1.11960507988E-02
F	-8.66618495552E+00	K	-1.51853098780E+00
G	-5.83137822089E+01	L	5.05192300379E-01
H	-6.97163410850E+01	M	7.09014109735E-02
I	-8.20099102783E+00	N	5.23899182335E-03
J	2.07195569008E+01	O	1.55103224352E-04
Y	6.74700000000E-01	Q	7.69602566960E+00
C <sub>V</sub>	4.00000000000E-01	R	-5.08857014030E-01
V <sub>0</sub>	6.41025640000E-01	S	9.13221006510E-02
$\alpha$	0.	T	2.18724108030E-02
A	-3.42126449447E+00	U	-7.72421839808E-03
B	-2.44309884639E+00	C <sub>V</sub>	5.00000000000E-01
C	2.26337419475E-01	Z	1.00000000000E-01

VTQ

C	1.98000000000E-01	D	-3.84065208171E-02
S	2.23000000000E+00	E	1.81393039475E-03
F	5.82606573241E-01	K	-1.56687680661E+00
G	-1.30770444275E+01	L	5.28664483962E-01
H	3.05673979749E+00	M	7.30767018647E-02
I	3.06801060993E+01	N	5.30349447649E-03
J	2.13250350559E+01	O	1.43461617399E-04
Y	1.50000000000E+00	Q	7.92725310775E+00
C <sub>V</sub>	3.30000000000E-01	R	-4.74542294271E-01
V <sub>0</sub>	5.39956803456E-01	S	1.20944307504E-01
$\alpha$	1.76000000000E-04	T	-1.74893025065E-02
A	-3.58647450079E+00	U	9.33856817842E-04
B	-2.29146630829E+00	C <sub>V</sub>	5.00000000000E-01
C	3.11339201717E-01	Z	1.00000000000E-01

Composition B

C	2.47000000000E-01	D	3.04510424546E-03
S	1.88000000000E+00	E	-1.75226403100E-01
F	-6.67122275062E+00	K	-1.56087684485E+00
G	-6.54470724004E+01	L	5.33121475935E-01
H	-1.26689986425E+02	M	8.06310874142E-02
I	-1.03958493089E+02	N	3.33816891056E-03
J	-2.82360096898E+01	O	-6.84399991171E-04
Y	1.32500000000E+00	Q	7.50278058550E+00
C <sub>V</sub>	3.30000000000E-01	R	-4.41209000835E-01
V <sub>0</sub>	5.83090379009E-01	S	1.51292636188E-01
$\alpha$	5.00000000000E-05	T	6.77883292739E-02
A	-3.52584878974E+00	U	-2.42403364371E-02
B	-2.33429189056E+00	C <sub>V</sub>	5.00000000000E-01
C	5.97267325606E-01	Z	1.00000000000E-01

## APPENDIX B

### BURN MODELS

#### I. FOREST FIRE BURN RATE

The mass fraction of unburned explosive  $W$  is defined as  $W = 1$  for a pure solid. The explosive burns to gaseous products with  $W = 0$  according to a pressure-dependent rate law based on experimental data.<sup>3,5</sup> The rate  $R$  is defined for pressure  $P$  in millibars and time  $t$  in microseconds by:

$$R = (1/W)(dW/dt)$$

$$\ln R = \sum_{i=1}^N C_i P^{i-1} .$$

The limiting conditions set  $R = 0$  for  $P$  less than a specified cutoff pressure and  $R = \infty$  ( $W \rightarrow 0$  immediately) when  $P$  reaches the C-J pressure. The rate parameters used in this study are tabulated in Table B-I.

These Forest Fire parameters are derived from the experimentally determined Pop plots. The equation of the Pop plot is

$$\ln x = A + B \ln P ,$$

with the run distance  $x$  in centimeters and the pressure  $P$  in millibars. The parameters are given in Table B-II.

#### II. C-J VOLUME BURN

The C-J volume burn model was used for pentolite. It assumes that  $W$  varies linearly with  $V$  from  $V_0$  to  $V_{CJ}$ . Proceeding from cycle  $n - 1$  to cycle  $n$ ,

$$W^n = 1 - \frac{V_0 - V^n}{V_0 - V_{CJ}} ,$$

where

$$1 \geq W^n \geq 0 , \quad W^n \leq W^{n-1} .$$

$$W^n = 0 \text{ if } W^n > W^{n-1} \text{ and } W^n < 0.7 .$$

$$P^n = (1 - W^n)P' ,$$

where  $P'$  is pressure of detonation products at V, I, and  $W = 0$ , if  $W^n < 0.99$ ; otherwise  $P'$  is  $P_0$ .  $V_{CJ} = 0.4723$  for the pentolite of this study. The other terms are defined in Appendix A.

TABLE B-I  
FOREST FIRE RATE PARAMETERS

PBX-9205

C-J PRESSURE = .281      CUT-OFF PRESSURE = .004

$c(i=1,14) = -1.1482508963e+01$	$7.1380350444e+02$	$-3.6528119877e+04$
$1.3178689915e+06$	$-3.1945087660e+07$	$5.3097654767e+08$
$-6.1811627328e+09$	$5.1077261600e+10$	$-3.0070047026e+11$
$1.2510375842e+12$	$-3.5904713587e+12$	$6.7580816604e+12$
$-7.5037456978e+12$	$3.7237130564e+12$	

PBX-9404

C-J PRESSURE = .363      CUT-OFF PRESSURE = .005

$c(i=1,14) = -8.3979132644e+00$	$4.0524452315e+02$	$-1.2887959724e+04$
$2.9889932207e+05$	$-4.7962436917e+06$	$5.4017707404e+07$
$-4.3377143285e+08$	$2.5068548091e+09$	$-1.0433258901e+10$
$3.0950369616e+10$	$-6.3781135352e+10$	$8.6704208069e+10$
$-6.9876089170e+10$	$2.5277953727e+10$	

TATB

C-J PRESSURE = .290      CUT-OFF PRESSURE = .010

$c(i=1,15) = -1.3725267870e+01$	$3.8903919286e+02$	$-5.1670574925e+03$
$-1.0249579222e+05$	$6.8977840930e+06$	$-1.6903862124e+08$
$2.5215834553e+09$	$-2.5479485981e+10$	$1.8139651006e+11$
$-9.2160587455e+11$	$3.3252111180e+12$	$-8.3244589903e+12$
$1.3746199680e+13$	$-1.3462111788e+13$	$5.9207965772e+12$

VTQ

C-J PRESSURE = .302      CUT-OFF PRESSURE = .003

$c(i=1,15) = -1.2831444411e+01$	$9.6584620364e+02$	$-6.1185473706e+04$
$2.6712441692e+06$	$-7.7485548201e+07$	$1.5372816488e+09$
$-2.1447556268e+10$	$2.1453404523e+11$	$-1.5541928421e+12$
$8.1584811109e+12$	$-3.0698283005e+13$	$8.0642956281e+13$
$-1.4035295599e+14$	$1.4535257742e+14$	$-6.7778693967e+13$

TABLE B-I (cont)

Composition B

C-J PRESSURE = .284

CUT-OFF PRESSURE = .005

$c(i=1,15) =$	$-1.0548089845e+01$	$7.5406695030e+02$	$-4.3585126588e+04$
	$1.7738926129e+06$	$-4.9055755777e+07$	$9.4323754961e+08$
	$-1.2896982914e+10$	$1.2736970319e+11$	$-9.1544370940e+11$
	$4.7819664606e+12$	$-1.7936038568e+13$	$4.7000815598e+13$
	$-8.1592157670e+13$	$8.4216539355e+13$	$-3.9083777111e+13$

TABLE B-II

## POP PLOT PARAMETERS

	<u>A</u>	<u>B</u>
PBX-9205	-4.384168	-1.501545
PBX-9404	-5.040996	-1.365368
TATB	-5.61223	-2.47086
VTQ-2	-5.263	-1.706
Composition B	-3.42995	-1.13388

## REFERENCES

1. Donna Price, A. R. Clairmont, Jr., and J. O. Erkman, "The NOL Large Scale Gap Test. III. Compilation of Unclassified Data and Supplementary Information for Interpretation of Results," Naval Ordnance Laboratory report NOLTR 74-40 (March 1974).
2. M. J. Urizar, S. W. Peterson, and L. C. Smith, "Detonation Sensitivity Tests," Los Alamos Scientific Laboratory report LA-7193-MS (April 1978).
3. C. L. Mader, Numerical Modeling of Detonations (University of California Press, Berkeley, 1979).
4. J. D. Kershner and C. L. Mader, "2DE, A Two-Dimensional Continuous Eulerian Hydrodynamic Code for Computing Multicomponent Reactive Hydrodynamic Problems," Los Alamos Scientific Laboratory report LA-4846 (March 1972).
5. C. L. Mader and C. A. Forest, "Two-Dimensional Homogeneous and Heterogeneous Detonation Wave Propagations," Los Alamos Scientific Laboratory report LA-6259 (June 1976).
6. C. L. Mader, "FORTRAN BKW: A Code for Computing the Detonation Properties of Explosives," Los Alamos Scientific Laboratory report LA-3704 (July 1967).
7. J. O. Erkman, D. J. Edwards, A. R. Clairmont, Jr., and Donna Price, "Calibration of the NOL Large Scale Gap Test: Hugoniot Data for Polymethyl Methacrylate," Naval Ordnance Laboratory report NOLTR 73-15 (April 1973).
8. R. Chéret, "Theoretical Considerations on the Propagation of Shock and Detonation Waves," 4th Internat. Symp. on Detonation, ACR-126, 78 (1965).
9. G. Taylor, "The Dynamics of the Combustion Products Behind Plane and Spherical Detonation Fronts in Explosives," Proc. Roy. Soc. A200, 235 (1950).